

*promoting access to White Rose research papers*



**Universities of Leeds, Sheffield and York**  
**<http://eprints.whiterose.ac.uk/>**

---

This is an author produced version of a paper published in **Geophysics**  
White Rose Research Online URL for this paper:

<http://eprints.whiterose.ac.uk/id/eprint/77389>

---

**Paper:**

Angus, DAC, Verdon, JP, Fisher, QJ and Kendall, J-M (2009) *Exploring trends in microcrack properties of sedimentary rocks: An audit of dry-core velocity-stress measurements*. *Geophysics*, 74 (5). E193 - E203. ISSN 0016-8033

<http://dx.doi.org/10.1190/1.3183940>

---

# Exploring trends in microcrack properties of sedimentary rocks: An audit of dry core velocity–stress measurements

*D. A. Angus<sup>1</sup>, J. P. Verdon<sup>2</sup>, Q. J. Fisher<sup>1</sup> & J–M. Kendall<sup>2</sup>*

*<sup>1</sup>School of Earth & Environment, University of Leeds, Leeds, UK*

*<sup>2</sup>Department of Earth Sciences, University of Bristol, Bristol, UK*

## ABSTRACT

Rock physics models are being used increasingly to link fluid and mechanical deformation parameters for dynamic elastic modelling. In this paper, we explore the input parameters of an analytic stress dependent rock physics model. To do this, we invert for the stress dependent microcrack parameters of over 150 sedimentary rock velocity–stress core measurements taken from a literature survey. The inversion scheme is based on a microstructural effective medium formulation defined by either a second–rank crack density tensor (scalar crack model) or both a second– and fourth–rank crack density tensor (joint inversion model). The inversion results are then used to explore and predict the stress dependent elastic behavior of various sedimentary rock lithologies using an analytic microstructural rock physics model via the initial model input parameters: initial crack aspect ratio and initial crack density. Estimates of initial crack aspect ratio are consistent between most lithologies with a mean of 0.0004, but for shales differ by up to several times in magnitude with a mean of 0.001. Estimates of initial aspect ratio are relatively insensitive to the inversion method, though the scalar crack inversion become less reliable at low values of normal to tangential crack compliance ratio ( $B_N/B_T$ ). Initial crack density is sensitive to the degree of damage as well as the inversion procedure. An important implication of this paper is that the fourth–rank crack density term is not necessarily negligible for most sedimentary rocks and evaluation of this term or  $B_N/B_T$  is necessary for accurate prediction of initial crack density. This is especially important since recent studies have suggested that the ratio  $B_N/B_T$  can be used as an indicator of crack fluid content.

## INTRODUCTION

Seismic monitoring of petroleum reservoirs has been used to image fluid compartmentalization and movement, stress redistribution as well as natural fracture distribution and hydraulic fracture formation. Time–lapse seismic monitoring is used to infer changes in pore pressure/stress and saturation within reservoirs and surrounding rock mass (e.g. Calvert, 2005). However, analysis of time–lapse results is complicated by the relative non–uniqueness of relating changes in seismic attributes (e.g., traveltime and acoustic impedance) to changes in reservoir fluid saturation and pore pressure. Although the interpretation of time–lapse seismic data is heavily influenced by reservoir complexity (e.g., geometry), a significant source of ambiguity in the seismic analysis stems from the uncertainty in relating perturbations in seismic velocities with stress/strain induced changes in the rock physical properties.

Recent studies have focused on applying coupled fluid–flow and geomechanical modelling for enhanced prediction of the subsurface response to fluid extraction and/or injection (e.g., Dean et al., 2005). Predicting the seismic response based on results from coupled fluid–flow and geomechanical modelling can be used to improve our understanding of the relationship between seismic attributes and changes in fluid properties, stress and mechanical deformation. However, this requires the use of rock physics models to link the fluid and mechanical properties of the reservoir system to so-called dynamic elastic (i.e., the elastic response suitable for seismic frequencies) models. Gassmann’s equation (see Brown and Korringa, 1975) is commonly used to explain relative changes in traveltimes and reflection amplitudes due to changes in fluid saturation. Yet fluid substitution alone has not been sufficient to explain the temporal and spatial changes in velocities, especially when mechanical deformation is occurring within the reservoir and surrounding rock mass (e.g., Hatchell and Bourne, 2005). This is because the elastic behavior of rock is observed also to be nonlinearly dependent on stress (e.g., Walsh, 1965a,b; Nur and Simmons, 1969).

Various approaches have been developed to account for the influence of stress and strain. For instance, Hatchell and Bourne (2005) derive a one-dimensional empirical formulation to link vertical traveltime perturbations to changes in vertical strain and velocity from time-lapse seismic data. Prioul et al. (2004) apply third-order elasticity (TOE) theory to develop an empirical nonlinear rock physics model capable of describing stress dependent elasticity and anisotropy. Bakulin et al. (2000), Shapiro (2003) and Shapiro and Kaselow (2005) provide nonlinear formulations derived from first-principal that are consistent with various empirically derived phenomenological equations (e.g., Zimmerman et al., 1986).

Only recently have nonlinear rock physics models been applied to coupled fluid–flow and geomechanical simulation to predict seismic attributes (e.g., Olden et al., 2001). Herwanger and Horne (2005) apply the empirical model of Prioul et al. (2004) to coupled flow–geomechanical simulation results and predict seismic anisotropy related to reservoir production stress perturbations. Angus et al. (2008) apply the analytic microstructural model of Verdon et al. (2008) to predict the influence of fault transmissibility on seismic velocities and stress induced seismic anisotropy. However, in these studies, the stress-dependent behavior of the dynamic elasticity is based on a limited number of field/core data.

In this paper, we examine the input parameters of the analytic microstructural stress dependent model of Verdon et al. (2008). The analytic formulation is an extension and adaption of the works of Tod (2002), Sayers (2002) and Hall et al. (2008). This approach is similar to TOE theory, except that the data are fitted to an exponential curve rather than two linear regimes at low and high effective stresses. The model is formulated in terms of an effective medium of idealized penny-shaped microcracks with initial crack density and initial aspect ratio, and can be applied to predict stress-induced elastic anisotropy as well as nonlinear and non-hysteretic elasticity. Specifically, we explore crack properties of the analytical microstructural rock physics model using laboratory measurements of ultrasonic velocities versus stress of dry core samples. We examine trends for various sedimentary rock lithologies to constrain the initial input parameters of the microstructural rock physics model. We also explore the ratio of crack normal to tangential compliance and how this parameter affects our estimates of the initial input parameters of the microstructural model. Establishing appropriate ranges of initial input parameters is essential for constructing dynamic elastic models from coupled fluid–flow and geomechanical simulation models.

## ROCK PHYSICS MODEL

### Theoretical background

Sayers and Kachanov (1995) model the influence of stress dependent elasticity due to the deformation of microcracks using the excess compliance approach of Schoenberg and Sayers (1995). The elastic anisotropy and stress dependence is expressed in terms of an excess compliance given by

$$\Delta S_{ijkl} = \frac{1}{4} (\delta_{ik}\alpha_{jl} + \delta_{jk}\alpha_{il} + \delta_{il}\alpha_{jk} + \delta_{jl}\alpha_{ik}) + \beta_{ijkl}, \quad (1)$$

where  $\delta_{ij}$  is the Kronecker delta. [Note that summation convention is used for equations 1–4]. The second- and fourth-rank crack density tensors  $\alpha_{ij}$  and  $\beta_{ijkl}$  are expressed

$$\alpha_{ij} = \frac{1}{V} \sum_m B_T^m n_i^m n_j^m S^m \quad (2)$$

$$\beta_{ijkl} = \frac{1}{V} \sum_m (B_N^m - B_T^m) n_i^m n_j^m n_k^m n_l^m S^m. \quad (3)$$

$B_N^m$  and  $B_T^m$  are the normal and tangential compliances across a microcrack (i.e., discontinuity surface)  $m$  having unit normal  $\mathbf{n}$  and surface area  $S^m$ . Thus the effective compliance  $S_{ijkl}$  of a rock can be expressed

$$S_{ijkl} = S_{ijkl}^0 + \Delta S_{ijkl}, \quad (4)$$

where  $S_{ijkl}^0$  is the background (or intact) rock compliance estimated from the mineral composition (Kendall et al., 2007) or behavior at high effective stresses (Sayers, 2002). The main assumptions in deriving these expressions are that the microcracks be rotationally invariant and thin. Although equations 1–4 describe the excess compliance of cracks (e.g., Sayers, 2002; MacBeth, 2004; Hall et al., 2008), we seek an analytic formulation based on physically intuitive input parameters to forward model the nonlinear stress dependence of elasticity (and hence seismic velocities) due to the presence of cracks.

### Analytic non-linear model

To construct dynamic elastic models from coupled fluid-flow/geomechanical models, we require an analytic rock physics model that can be calibrated using core data and has minimal initial input parameters. Verdon et al. (2008) apply the analytic effective medium formulation of Tod (2002) to predict the anisotropic and stress dependent seismic velocities presented in Hall et al. (2008). This analytical model is formulated in terms of a stress dependent second-rank crack density tensor as well as crack aspect ratio to predict elastic anisotropy and stress dependence. The crack number density is expressed (hereafter referred to as crack density)

$$\epsilon_i(\sigma_{ii}^e) = \epsilon_i^0 \exp[-c_i^r \sigma_{ii}^e] \quad (5)$$

where

$$c_i^r = \frac{1}{\pi \mu_i a_i^0} \left( \frac{\lambda_i + 2\mu_i}{\lambda_i + \mu_i} \right), \quad (6)$$

$\lambda_i$  and  $\mu_i$  are the Lamè constants and  $\sigma_{ii}^e$  is the principal effective stress in the  $i$ -th direction, and  $\epsilon_i^0$  and  $a_i^0$  are the effective initial crack density and effective initial aspect ratio, respectively. [Hereafter we do not use the term effective in describing initial crack density and initial aspect ratio. Later we explain why the qualifier ‘effective’ is introduced for these initial model parameters.] The second-rank microcrack density term is

$$\alpha_{ii} = \frac{\epsilon_i}{h_i} \quad \text{where} \quad h_i = \frac{3E_i^0[2 - \nu_i^0]}{32[1 - (\nu_i^0)^2]} \quad (7)$$

is a normalization factor (Schubnel and Guéguen, 2003), and  $E_i^0$  and  $\nu_i^0$  are the anisotropic intact rock Young’s modulus and Poisson’s ratio. [Note that summation convention is not implied for equations 5–7]. This derivation yields an expression for the effective elasticity that can model stress-induced anisotropy and nonlinearity due to deviatoric stress fields. It should be noted that this model does not model the behavior of rock undergoing plastic or brittle deformation. Assuming penny-shaped cracks, where  $\beta_{ijkl} = 0$  (see next section), and incorporate equation 7 into 1, the effective compliance predicted by the analytic rock physics model is given by equation 4.

The necessary input parameters for the microstructural stress-dependent dynamic elasticity model are the background stiffness ( $S_{ijkl}^0 = 1/C_{ijkl}^0$ ), triaxial effective stress tensor ( $\sigma_{ij}$ ), and the initial crack density and aspect ratio ( $\epsilon_i^0$  and  $a_i^0$ ). Since coupled flow-geomechanical simulations supply the effective stress tensor, background stiffness and density, the microstructural rock physics model can be incorporated with the coupled flow-geomechanical simulation to construct dynamic elastic (i.e., seismic) models for seismic modeling applications. However, the initial crack density and aspect ratio remain poorly constrained.

Verdon et al. (2008) estimate the initial crack density and aspect ratio of several sandstone samples from the Clair reservoir (Kendall et al., 2007) and several thermally damaged sandstone samples (MacBeth and Schuett, 2007). The inversion results show initial crack densities ranging between approximately  $\epsilon^0 \in (0.08, 0.8)$  and initial aspect ratios ranging between  $a^0 \in (0.0005, 0.005)$ . The inversion results for the thermal damage experiment of MacBeth and Schuett (2007) confirm the expected result that the initial crack density term is sensitive to core damage. Although qualitatively instructive, the range of values obtained from a limited number of sandstone samples is not statistically compelling. This is especially important if the nonlinear rock physics model is to be linked with coupled flow-geomechanical simulation to predict the seismic response of a producing reservoir. Thus, it is necessary to seek improved constraints on the range of acceptable initial crack densities and aspect ratios from a greater number of core samples as well as various lithologies.

## CALIBRATION OF ROCK PHYSICS MODEL

Sayers (2002) and Hall et al. (2008) apply equations 1–4 to invert for the nonlinear elasticity tensor. In both studies, they find that reasonably accurate estimates of the stress dependent velocities can be obtained using only the second-rank crack density term  $\alpha_{ij}$ . Hall et al. (2008) further invert for the fourth-rank density term  $\beta_{ijkl}$ , but under the assumption that  $\beta_{ijkl}$  is small and due solely to the misfit between the data and the second-rank term  $\alpha_{ij}$ . Verdon et al. (2008) also perform a joint inversion for  $\alpha_{ij}$  and  $\beta_{ijkl}$  without assuming *a priori* that  $\beta_{ijkl}$  is small. The results from both Hall et al. (2008) and Verdon et al. (2008),

using a limited data set, suggest that the magnitude of  $\beta_{ijkl}$  is such that the scalar crack assumption (see discussion to follow) is a reasonable approximation.

To constrain the input parameters of the analytic microstructural rock physics model, we apply the approach of Verdon et al. (2008) to evaluate the excess compliance of stress versus ultrasonic velocity measurements of dry core samples. First, we perform a ‘scalar crack inversion’, where we invert only for the second-rank crack density term given by equation 2 and assume the fourth-rank term given by equation 3 is negligible ( $\beta_{ijkl} = 0$ ). Second, we perform the ‘joint inversion’, where we invert for both the second- and fourth-rank crack density terms. We subsequently use the inverted second-rank density term (equation 2) to solve for the best fitting initial crack density  $\epsilon^0$  and initial aspect ratio  $a^0$  via equations 5–7. To recapitulate, the scalar crack and joint inversions assume only that the microcracks are rotationally invariant and thin. However, when solving for the best fitting initial crack density and aspect ratio, we assume also that the microcracks are penny-shaped to introduce a measure of crack aspect ratio. The flowchart in Figure 1 describes the workflow to evaluate the best fitting input parameters  $\epsilon^0$  and  $a^0$  of the analytic microstructural model.

### Significance of $\beta_{ijkl}$

Before discussing the results of the inversions, it is useful to consider the significance of the fourth-rank crack density term. For most rocks, the fourth-rank term  $\beta_{ijkl}$  is often assumed negligible and only the contribution from the second-rank term  $\alpha_{ij}$  is thought sufficient in describing the nonlinear stress dependent elasticity (Grechka and Kachanov, 2006; Hall et al., 2008; Verdon et al., 2008). For small values of  $\beta_{ijkl}$  and assuming penny-shaped cracks, the ratio of crack normal to tangential compliance  $B_N/B_T$  is approximately one. The so-called scalar crack assumption refers to the special case when  $B_N/B_T = 1$ . With the scalar crack assumption, the excess compliance due to a distribution of penny-shaped displacement discontinuities can be assessed by considering only contributions of the three diagonal components of  $\alpha_{ij}$ . Thus  $\alpha_{ij}$  can be used to describe the orientation and density of three mutually orthogonal sets of aligned microcracks. For example, Sayers and Kachanov (1995) note that for the Berea sandstone the Poisson’s ratio ranges between  $0.1 < \nu < 0.2$  and for such a case, using only the second-rank crack density tensor  $\alpha_{ij}$  can yield a reasonable approximation of the rock stress sensitivity. This is because when the Poisson’s ratio is small  $\beta_{ijkl}$  is an order of magnitude smaller than  $\alpha_{ij}$ . However, the Poisson’s ratio for sedimentary rocks typically range anywhere between  $0.1 \leq \nu \leq 0.4$ . Thus for larger values of Poisson’s ratio, the assumption of penny-shaped and scalar cracks may not be the most appropriate assumption for estimating the behavior of all reservoir rocks.

Various mathematical expressions exist for representing the ratio of normal to tangential compliance of a discontinuity surface (e.g., crack), such as

$$\frac{B_N}{B_T} = \left(1 - \frac{\nu}{2}\right) \quad \text{and} \quad \frac{B_N}{B_T} = \left(\frac{1 - \nu}{1 - \nu/2}\right) \quad (8)$$

for a planar distribution of drained small isolated cracks and drained rough surfaces (Lubbe et al., 2008), respectively. For  $\nu \in (0.1, 0.4)$ , one would predict the range of the  $B_N/B_T$  ratio for dry (or gas filled) discontinuities to be (0.75, 0.95). However, recent laboratory estimates of  $B_N/B_T$  ratio for sandstone (MacBeth and Schuett, 2007) and limestone (Lubbe

et al., 2007, 2008) dry core samples have found values significantly lower than unity, with ratios ranging between 0.0 and 0.6. MacBeth and Schuett (2007) also note that for (thermally) damaged samples the ratio may increase to values above unity. Deviations from the scalar crack assumption potentially result from several factors, such as the presence of fluids with non-zero bulk modulus, cement or clay within cracks as well as more complex crack geometries (i.e., non-idealized penny-shaped cracks). Later in this paper, we show that  $B_N/B_T$  for sedimentary rocks is on average less than unity and that the scalar crack assumption is generally not valid.

## RESULTS

In this section, we apply the approach described in the previous section on over 150 ultrasonic velocity versus stress dry core measurements from various published studies as well as graduate theses (data were compiled from the studies listed in Table 1). The results are examined for any lithologic and depth dependence of the initial crack density  $\epsilon^0$  and initial aspect ratio  $a^0$ , which may provide important initial constraints. Results from the joint inversion are used to examine the significance of  $\beta_{ijkl}$  on the evaluation of  $\epsilon^0$  and  $a^0$  as well as to explore the range of estimated  $B_N/B_T$  ratios. Finally, we examine the errors introduced in estimating the initial input parameters ( $\epsilon^0$  and  $a^0$ ) of the analytic microstructural rock physics model by inverting for only  $\alpha_{ij}$  when  $B_N/B_T \neq 1$  using synthetically generated data.

In compiling the data, all velocity measurements were converted into an elastic tensor, where the symmetry of the elastic tensor was determined by the number of available directionally independent P- and S-wave measurements. When only one P- and one S-wave velocity were available, the elastic tensor was assumed isotropic. Since the majority of the results were isotropic (i.e., generally only one P- and one S-wave measurements were available), all anisotropic elastic tensors were converted to an isotropic equivalent tensor to allow a global comparison of all inversion results. Evaluation of the isotropic equivalent of an anisotropic elastic tensor was performed using a Voigt-Reuss-Hill directional averaging approach (Kendall et al., 2007). However, it is important to stress that our rock physics model is not restricted to isotropy. Not only can the background elasticity (or compliance) be anisotropic, but directionally dependent velocity measurements can be utilized to evaluate anisotropy in initial crack density and initial aspect ratio.

### Scalar crack inversion ( $\alpha_{ij}$ only)

*All samples:*

Figure 2 displays initial crack density  $\epsilon^0$  versus initial aspect ratio  $a^0$  estimates from the scalar crack inversion procedure for all the dry core samples. Also shown (inset) are histograms for  $\epsilon^0$  and  $a^0$ . In this figure, the initial aspect ratios show some scatter but there is a remarkable clustering with mean of approximately  $\bar{a}^0 = 0.0004$ . This result is consistent with the aspect ratio inversion of King (2002) for a Crosland Hill sandstone sample (the effective medium model consists of sets of aligned oblate spheroidal discontinuities having transversely isotropic symmetry). The initial crack density estimates in Figure 2 show much more scatter, falling between  $\epsilon^0 \in (0.0, 0.5)$  and having mean  $\bar{\epsilon}^0 = 0.1$ . There appears to be

no systematic trend for lithology, except that the shale and limestone samples have initial aspect ratios ranging between approximately  $a^0 \in (0.001, 0.004)$ , greater than the global trend of the dry samples. Table 2 summarizes the mean estimates for various lithologies for both  $\epsilon^0$  and  $a^0$ . The initial aspect ratio of shale differs significantly from the other lithologies being approximately twice in magnitude. Both the sandstone and tight-gas sandstone lithologies have initial crack densities of approximately 0.15, whereas the shales and carbonates have values of 0.04 and 0.08, respectively.

We also examined the initial crack density and initial aspect ratio with depth and porosity, but noticed no observable trends. However, it should be noted that the majority of the core samples were taken either from surface outcrops or reservoir depths. Thus the limited depth distribution in the data is not sufficient to extract any depth and porosity trends in  $\epsilon^0$  and  $a^0$ .

Although shales are very abundant in reservoir systems, there is relatively little known about their geomechanical properties, primarily due to their fine grain size and, until recently, lack of interest from hydrocarbon production programs. Shales represent a broad class of siliciclastic rocks and generally encompass any rock with greater than 50 % clay content. Since it has been observed that shales behave mechanically quite different from sandstones, it is instructive to examine the inversion results in terms of individual lithologies.

In Figure 3, initial crack density versus aspect ratio are plotted for two separate lithologies: (a) sandstones and (b) clay rich samples. The inset within both are histograms for  $\epsilon^0$  and  $a^0$ . For the sandstone samples (Fig. 3a), initial aspect ratio estimates cluster tightly around 0.0004, with significant variation in initial crack density ranging between 0 and 0.5. In Figure 3b,  $a^0$  shows significant scatter and  $\epsilon^0$  less scatter for the clay rich samples. For the ‘pure’ shale samples, only three fall within the range of the initial aspect ratio global average – these are the Mannville shale core samples provided by Hemsing (2007). The Mannville shales consist largely of quartz with a significant amount of clay content. However, the clay content within these three samples is on the lower end of typical shales (Hemsing, 2007) and this may explain why the estimated initial aspect ratios for these shaley sandstones are similar to those of the global trend (i.e., sandstones). The tight-gas shale samples (taken from Jizba, 1991) also display initial aspect ratio estimates sensitive to clay content consistent with the pure shale samples. Also shown in Figure 3b are the Clair sandstone estimates (gray triangles labeled B, C, D, E, F, and I) for comparison and their significance will be discussed below.

### *Clair sandstone samples*

One issue with analyzing data compiled from various published sources is that experimental procedure and equipment can vary significantly from study to study as well as with time. Furthermore, the core sample observations provided can be limited (e.g., only density, porosity, velocities and effective stresses). Access to detailed core sample description can provide valuable information to complement ultrasonic velocity measurements, which are often not available in published studies. Thus we are limited to general conclusions based on global trends.

Measurements of the reservoir sandstone core samples from the Clair Field obtained

during the SAIL (Seismic Anisotropy as an Indicator of Lithology) consortium project (see Kendall et al., 2007) represent a subset of the compiled data that provide additional core physical properties available to the authors. For each of these samples, there are detailed petrophysical analysis, such as quantitative X-ray diffraction for mineralogical analysis of the mineral constituents, electron back-scattered diffraction (EBSD) to characterize the orientation of quartz, feldspar and calcite grains, and X-ray texture goniometry and image analysis to evaluate crystal preferred orientation (CPO) of mica and clay grains.

Table 3 shows various sample physical properties for the six Clair sandstone samples and the estimated initial crack density and initial aspect ratio (see labeled gray triangles in Figure 3). Samples E, F and I represent clean sandstone samples and show initial aspect ratios consistent with the general trend of all the sandstone samples, but with significant variation in initial crack densities. Sample E has been chemically cleaned and so may be more representative of a damaged sample. Samples B, D and C have increasing clay content (roughly 12%, 30% and 35%), but still show initial aspect ratios consistent with the general trend of all sandstones. However, sample C has the highest clay content and also displays the greatest initial aspect ratio. It is difficult to conclude with any certainty from the Clair sandstones alone that increasing clay content leads to increasing initial aspect ratio. Interpretation of the behavior of the Clair sandstones might be affected by the fact that the Clair field has undergone significant uplift during its geological evolution. Furthermore, the stress-velocity data for these samples deviate to varying degrees from the typical exponential stress sensitivity with increasing pressure typical of most sedimentary rocks. However, the results from the shale samples as well as the Clair sandstones together suggest that there might be a relation between clay and mica content and initial aspect ratio. More velocity-stress data for shales and shaley (clay rich) sandstones, with accompanying petrophysical analyses, are necessary to study the potential link between shale content and increasing aspect ratio.

To understand how mica and clay might influence estimates of the initial aspect ratio it is helpful to examine the microstructure of the clean and shaley sandstones. In Figure 4, EBSD images are shown for the clean sandstone sample F and I, and the shaley sandstone sample C. The microstructure of the clean sandstone samples show remarkable consistency in orientation of quartz and feldspar grains associated with paleoflow, whereas the calcite and dolomite grains show random orientation as a result of their diagenetic origin (Valcke et al., 2006). The EBSD image of the shaley sample C shows a CPO of the mica-clay grains with vertical symmetry due to mechanical compaction. The orientation of the quartz and feldspar grains are similar to those of the clean samples. Comparing the microstructural images of the clean sandstones with the shaley sandstone highlights the dominance of the mica and clay grains. The dominance of the clay rich minerals is also observed in the seismic anisotropy analysis of Kendall et al. (2007), where the presence of up to 20% to 40% mica and clay grains leads to a dominant vertical transverse isotropy (VTI) signature. However, it is not clear how large an influence this strong lithologic anisotropy plays on the initial aspect ratio estimates and further study is necessary. For example, does this initial VTI skew the inversion estimates of initial aspect ratios or does the presence of significant amounts of mica and clay grains lead to an inherent microstructural bias of physically larger microcrack aspect ratio?

### Full inversion ( $\alpha_{ij}$ and $\beta_{ijkl}$ )

Figure 5 shows the results of the over 150 initial crack density  $\epsilon^0$  versus initial aspect ratio  $a^0$  estimates using the joint inversion procedure. Also shown (inset) are the histograms for both  $\epsilon^0$  and  $a^0$ . The general trend within this figure is comparable to that of Figure 2. The behavior of  $a^0$  appears similar, but with the few outlying data points falling much further away from the general trend. In terms of initial crack density, the scatter increases as seen in the broader distribution in the inset histogram.

Table 4 summarises the mean estimates for various lithologies for both  $\epsilon^0$  and  $a^0$ . The initial aspect ratio of shale again differs significantly from the other lithologies being approximately twice in magnitude. As well, the inversion for  $a^0$  seems to be insensitive to the magnitude of  $\beta_{ijkl}$  suggesting that inverting for only  $\alpha_{ij}$  can yield consistent estimates of initial aspect ratio. The sandstone, tight-gas sandstone and carbonate lithologies all have similar order of magnitude initial crack densities of approximately 0.12 to 0.14, whereas the shale lithology has a value of 0.02. It should be noted that the misfit between observed and predicted elasticity improves with the joint inversion. This is an expected result as including the fourth-rank tensor within the inversion allows the influence of crack normal compliance to be modeled. In general, this suggests that the results from the joint inversion should provide a more reliable description of the microcrack characteristics.

In Figure 6, initial crack density versus aspect ratio are plotted again for two separate lithologies: (a) sandstones and (b) clay rich samples. Inset within both are histograms for  $\epsilon^0$  and  $a^0$ . For the sandstone samples (Fig. 6a), initial aspect ratio estimates cluster tightly around 0.0004, with significant variation in initial crack density ranging between 0 and 0.9. For the clay rich samples (Fig. 6b),  $a^0$  shows slightly more scatter whereas the distribution is less diffuse for  $\epsilon^0$ . For the ‘pure’ shale samples, none of the samples fall within the range of the initial aspect ratio global average. However, the shale core samples as well as the tight-gas shale samples still display initial aspect ratio estimates sensitive to clay content.

Also shown in Figure 6b are the Clair sandstone  $\epsilon^0$  and  $a^0$  estimates (gray triangles labeled B, C, D, E, F, and I), where the percent clay content are known quantitatively for each sample. The clean sandstone samples B, I and F all have initial aspect ratios consistent with the sandstone lithology trend. The clay rich samples C and D as well as the chemically cleaned sandstone sample E all have initial aspect ratio larger than the sandstone average. For these samples, joint inversion for both  $\alpha_{ij}$  and  $\beta_{ijkl}$  only marginally improved the misfit between observed and predicted elasticity.

### Estimating the $B_N/B_T$ ratio

The joint inversion procedure for  $\alpha_{ij}$  and  $\beta_{ijkl}$  developed by Verdon et al. (2008) is formulated on the assumption that the microcracks are identically shaped (i.e., rotationally invariant) and thin, and that  $\beta_{ijkl}$  is isotropic to simplify the set of equations used in the inversion procedure. With the above assumptions, the fourth-rank tensor can be expressed in terms of the second-rank tensor

$$\beta_{1111} = \beta_{2222} = \beta_{3333} = \frac{1}{3} \left( \frac{B_N}{B_T} - 1 \right) \alpha^m \quad (9)$$

$$\beta_{1122} = \beta_{1133} = \beta_{2233} = \beta_{1212} = \beta_{1313} = \beta_{2323} = \frac{1}{3}\beta_{1111} , \quad (10)$$

where

$$\alpha^m = \text{trace}(\alpha_{ii}) \quad \text{and} \quad \alpha_{ii} = \frac{\pi N r^2}{3V} B_T \quad (11)$$

(Sayers and Han, 2002). The scalar  $N$  is the number of discontinuities in a volume  $V$  and  $r$  is the radius of the crack. Similar to Verdon et al. (2008), we perform a grid search over  $B_N/B_T$ , with a range of allowable values between  $B_N/B_T \in (0.0, 2.0)$ .

In Figure 7, histograms for  $B_N/B_T$  are shown for all lithologies as well as for the sandstone and carbonate samples. For all lithologies (Fig. 7 gray shaded), the estimate ratios span the entire range with the majority falling within approximately 0.4 and 1.5. It should be noted that the inversion for  $B_N/B_T$  is unstable at high confining stresses and so we disregard estimates at these stresses. The instability arises because we estimate the background compliance  $S_{ijkl}^0$  in equation 4 using the high stress compliance approach of Sayers (2002) (there is no information on the mineral compliance for most of the core data with which to estimate the background compliance  $S_{ijkl}^0$ ). As a result, when the effective stress approaches the highest stress, the estimated background compliance approaches the high stress compliance and leads to instability in the inversion procedure. Ratio estimates below 0.25 and above 1.75 are predominantly a result of either poor data or deviations from isotropic  $\beta_{ijkl}$ . The sandstone samples (Fig. 7 blue line) are characterized by  $B_N/B_T$  between 0.25 and 1.0, with a significant frequency around 0.6. The carbonate samples (Fig. 7 red line) also show similar characteristics, but with a slightly skewed distribution and peak around 0.55.

Figure 8 compares the  $B_N/B_T$  estimates for the sandstone (gray shaded) and tight-gas sandstone lithologies. For all the tight-gas sandstones of Jizba (1991) [Fig. 8 blue line], the distribution is much broader and skewed to higher ratios, with a weak peak around 0.75 and significant frequencies from up to 1.75. Focusing on the results from Rojas (2005) [Fig. 8 red line], the tight-gas samples have values between 0.25 and 1.25, and have similar  $B_N/B_T$  characteristics to those of the sandstone lithologies. However, those from Jizba (1991) differ significantly; possible reasons for this may be that the specific samples are poorly cemented or may have been damaged due to core extraction and/or reservoir production (e.g., hydraulically induced fracturing).

Figure 9 show the results for  $B_N/B_T$  estimates for the shale and tight-gas shale lithologies. The distribution for all shale samples (Fig. 9 gray shaded) and the shale samples of Hemsing (2007) [Fig. 9 red line] fall mainly within approximately 0.0 and 1.5. The results for the tight-gas shales (Jizba, 1991) [Fig. 9 blue line] are just as diffuse, with clusters around 0.6 and 1.5. However, since there are relatively limited data for the shales, it is difficult to draw any definitive conclusions other than that the range of  $B_N/B_T$  ratios can vary between 0.0 to 1.75.

For comparison, we estimate  $B_N/B_T$  using the velocity-stress data for the aeolian Rotliegend sandstone samples presented in Figures 3, 4 and 6 of MacBeth and Schuett (2007). The results for the undamaged samples (Fig. 10 gray shaded) show a distribution between 0.0 and 0.8, with mean of approximately 0.6. For the thermally damaged samples (Fig. 10 red line), we also observe an increase in the range of  $B_N/B_T$  ratios, with values between approximately 0.0 and 1.9. These results show some similarity with those of

MacBeth and Schuett (2007), Figure 7c, except that our estimated means are significantly larger. Potential sources of discrepancy between our results and those of MacBeth and Schuett (2007) are theoretical differences in methodology, errors introduced from digitizing the graphical data into discrete velocity versus stress data and applying the high stress assumption to estimate the background elasticity.

### **Errors introduced by inverting for $\alpha_{ij}$ only**

The results from the previous section clearly demonstrate that the scalar crack assumption is not consistent with the joint inversion results of the velocity–stress core data. This stresses the importance of inverting for both the second– and fourth–rank crack density terms for more accurate prediction of nonlinear elasticity, at least in terms of the initial crack density and initial aspect ratio. The question that arises is what effect does neglecting the fourth–rank tensor have on estimates of the initial crack density and initial aspect ratio for the nonlinear analytic rock physics model of Tod (2002). In this section, we perform a numerical test to examine the inversion results for the scalar crack assumption as well as for both  $\alpha_{ij}$  and  $\beta_{ijkl}$ .

A synthetic stress versus velocity data set is generated using a representative sedimentary anisotropic mineral elasticity (Raymer et al., 2000) as the background elasticity. The stress dependence is evaluated using equations 1–4 (see Sayers, 2002; Hall et al., 2008; Verdon et al., 2008), where  $\alpha_{ij}$  is determined by equation 7 and  $\beta_{ijkl}$  using the relations 9–10. A total of 84 synthetic core experiments are generated for a range of  $B_N/B_T \in (0.0, 2.0)$  at increments of 0.1 for four sets of initial crack density and initial aspect ratio:  $(\epsilon^0, a^0) = (0.1, 0.0005)$ ,  $(0.5, 0.0005)$ ,  $(0.1, 0.001)$  and  $(0.5, 0.001)$ . For the inversion procedure we use the high stress assumption to approximate the mineral elasticity for both the scalar crack and joint inversions.

Figure 11 shows the absolute errors of the scalar crack and joint inversions for the synthetic data set. For the initial crack density estimates (Fig. 11a), the joint inversions yield essentially identical estimates. This is to be expected since the only difference between the synthetic data and the estimated data is that the estimated data use the high stress compliance of the synthetic data as an estimate of the background elasticity and not the true mineral compliance. There is significant error for the scalar crack inversion, where only accurate estimates are obtained for inversions where synthetic data have  $B_N/B_T$  ratios close to unity. For low  $B_N/B_T$ ,  $\epsilon^0$  is underestimated, whereas it is overestimated for high  $B_N/B_T$ . This has important implications in the estimation and prediction of rock damage (i.e., induced fracturing) in terms of crack density estimates. For the initial aspect ratio (Fig. 11b), the joint inversion yields accurate inversions as expected. Although the scalar crack inversion produces accurate results for  $B_N/B_T$  ratios between approximately 0.7 and 1.6, it becomes less reliable for values below 0.4.

These results suggest that it is important to evaluate both the second– and fourth–rank tensors to properly estimate the initial parameters of the nonlinear rock physics model of Tod (2002). The results also indicate that a correction term may be necessary for this analytic model if the influence of the crack compliance ratio is significant. A first–order approach would be to introduce a stress independent fourth–rank term based on an average  $B_N/B_T$  ratio estimated from the core data. Thus, the stress dependent elasticity tensor

can be constructed using the crack density terms 7, 9–10 and equations 1–4.

## DISCUSSION

It is important to stress that although the microstructural nonlinear rock physics model is not a rigorous description of the true microstructure of sedimentary rock, it does provide an accurate means of predicting the averaging effects of the microstructure in terms of wave properties. Furthermore, this effective medium model is conceptually very attractive as it is formulated in terms of two initial parameters; effective initial crack density  $\epsilon^0$  and effective initial aspect ratio  $a^0$  which can be linked to rock microstructure. Referring back to equations 5–7, increasing initial crack density  $\epsilon^0$  will result in a weaker or more compliant rock. Although initial aspect ratio does not affect the overall strength of the rock, it does influence the stress sensitivity. For example, increasing initial aspect ratio leads to lower stress sensitivity of the elasticity at lower confining stresses.

How these effective medium parameters relate to real physical (mechanical) properties of the rock is not trivial. For real rock, an increase in crack density is most likely related to opening of existing cracks, generation of new grain boundaries and/or breakage of existing intergrain cement bonds. Thus the effective crack density represents a proxy for damage on the grain scale. The effective initial aspect ratio  $a^0$  is related to the shape of the non—equant porosity void space. Thus for real rock, the effective initial aspect ratio describes the average shape (or more dominant shape distribution) of the stress sensitive microcracks. Relating the effective medium estimate of microcrack normal to tangential compliance ratio  $B_N/B_T$  to the actual microcrack compliance behavior is more tenuous. However, the range of the estimated ratios (between 0.25 and 0.75, with mean of approximately 0.55) is consistent with discontinuities modeled as rough surfaces in contact under confining stresses (Palciauskas, 1992; MacBeth and Schuett, 2007). The estimated ratios for damaged samples fall predominantly between 0.25 and 1.75, where the microcracks of the thermally damaged samples are observed to have clean linear geometry (MacBeth and Schuett, 2007). Since planar surfaces are expected to have higher normal compliance than imperfect surfaces (i.e., smooth planar surfaces will have fewer asperities to resist closure), it is expected that clean, planar microcracks will have higher  $B_N/B_T$  ratios (MacBeth and Schuett, 2007). Furthermore, for fluid filled discontinuities, the  $B_N/B_T$  ratio would be altered due to the change in compressibility of the crack filling material, where the ratios are predicted to be lower (e.g., Sayers and Han, 2002; Worthington, 2008).

The influence of clays and fluids within microcracks as well as capillary forces has important implications on the stress sensitivity of rocks (Van Den Abeele et al., 2002). However, more research is needed to establish the links between mechanical properties of rocks with respect to clay, fluids and capillary forces. Specifically, how do clay minerals, fluids and capillary forces influence the microstructural rock physics model parameters: initial aspect ratio, initial crack density and  $B_N/B_T$ . Furthermore, the influence of fluids is particularly problematic in the measurement of elastic properties of so-called dry (or room dry) shale and clay rich core samples. This is because clay rich rocks are rarely completely dried due to, for example, the presence of strong capillary forces. If the samples were completely dried, it is likely that their microstructure and elastic properties would be irreversibly changed (Boris Gurevich, personal communication).

A key result of this study is the implication that estimating the second-rank crack den-

sity term assuming the fourth-rank tensor is negligible (i.e., the scalar crack assumption) can lead to large errors in estimating initial crack density  $\epsilon^0$  when the ratio of normal to tangential crack compliance deviates from unity. Specifically, full inversion for both the second- and fourth-rank crack density tensors is necessary to properly characterize the stress sensitivity of rock. This is particularly important if the inversion scheme is used to evaluate the input parameters for the nonlinear microstructural rock physics model. To routinely apply crack density as a proxy for damage, more analysis of core data is needed to quantify rock damage in terms of initial crack density. The ability to link damage to an effective crack density parameter would allow us to explore quantitative assessment of induced fracturing using techniques such as shear-wave splitting analysis. From a qualitative perspective, initial aspect ratio can be used as a proxy for the stress sensitivity of rock. Although aspect ratio varies with lithology, it remains relatively well constrained for sandstones, tight-gas sandstones and carbonates, but varies significantly for shales. Understanding why initial aspect ratio is significantly different for shales and relatively consistent for all other lithologies may allow us to better understand how the mechanical properties of shales affect seismic waves.

Measurement of rock physical properties of dry core samples provide valuable information on the elastic properties of sedimentary rocks. However, sedimentary rocks are seldom under ‘dry conditions’ and so more realistic characterization of rock physical properties should be examined under fluid saturated conditions (e.g., Han, 1986). Since it is expected that the dispersive effects of the fluid-filled cracks as well as viscosities of the saturating fluids can significantly effect velocity measurements at ultrasonic frequencies, extension of the inversion procedure to include the effects of squirt flow will be necessary. By incorporating an effective squirt flow model, we can explore the role that fluids may have on crack density, aspect ratio and the ratio  $B_N/B_T$ .

## CONCLUSION

In this paper we invert for the stress sensitive microcrack parameters of over 150 dry sedimentary core samples and evaluate the results in terms of a microstructural nonlinear rock physics model. From these results, the input parameters (initial crack density  $\epsilon^0$  and initial aspect ratio  $a^0$ ) are constrained on the basis of lithology. For most sedimentary lithologies, initial aspect ratios cluster tightly around 0.0004, and for clay rich lithologies around 0.001. The results for initial crack density are more diffuse and vary significantly between lithologies. This variation likely has more to do with core damage than lithological differences in the microstructure.

Estimates of the crack normal to tangential compliance indicate that for intact and damaged rocks the range of values is anywhere between  $0.0 < B_N/B_T < 2.0$ . The global trend suggests that  $B_N/B_T$  clusters around 0.6, which is also observed for both the sandstone and carbonate samples. The results for tight-gas sandstones and shales are more diffuse, with values ranging between approximately 0.1 to 1.9. Estimates from the intact and thermally damaged core samples are consistent with other published studies, showing that for intact rock  $B_N/B_T$  is lower than unity and that the range broadens and expands to values higher than unity when the rock is damaged.

## ACKNOWLEDGEMENTS

We thank ITF and the sponsors of the IPEGG project, BG, BP, Statoil and ENI. We also thank Colin Sayers for informal discussion of our results during the initial stages of this work as well as Associate Editor Boris Gurevich, Sonja Maultzsch and three anonymous reviewers for constructive criticism. James Verdon was supported by a UKERC Interdisciplinary Studentship Award. Doug Schmitt is also thanked for providing some of the data from his masters students. All figures were generated using GMT (Wessel and Smith, 1991).

## REFERENCES

- Angus, D., J. Verdon, J.-M. Kendall, Q. Fisher, J. Segura, S. Skachkov, M. Dutko, and A. Crook, 2008, Influence of fault transmissibility on seismic attributes based on coupled fluid–flow and geomechanical simulation: Annual International Meeting, Society of Exploration Geophysicists, Expanded Abstracts.
- Bakulin, A., I. Tsvankin, and V. Grechka, 2000, Estimation of fracture parameters from reflection seismic data—Part I: HTI model due to a single fracture set: *Geophysics*, **65**, 1788–1802.
- Brown, R. and J. Korrington, 1975, On the dependence of the elastic properties of a porous rock on the compressibility of the pore fluid: *Geophysics*, **40**, 608–616.
- Brown, L., 2002, Integration of rock physics and reservoir simulation for the interpretation of time–lapse seismic data at Weyburn Field, Saskatchewan: Master’s thesis, Colorado School of Mines.
- Calvert, R., 2005, Insights and methods for 4D reservoir monitoring and characterization: Society of Exploration Geophysicist.
- Dean, R., X. Gai, C. Stone, and S. Minkoff, 2005, A comparison of techniques for coupling porous flow and geomechanics: Society of Petroleum Engineering Reservoir Simulation Symposium, page 79709.
- Grechka, V. and M. Kachanov, 2006, Effective elasticity of fractured rocks: *The Leading Edge*, **25**, no. 2, 152–155.
- Grochau, M. and B. Gurevich, 2008, Investigation of core data reliability to support time–lapse interpretation in Campos Basin, Brazil: *Geophysics*, **73**, no. 2, E59–E65.
- Hall, S., J.-M. Kendall, J. Maddock, and Q. Fisher, 2008, Crack density tensor inversion for analysis of changes in rock frame architecture: *Geophysical Journal International*, **173**, 577–592.
- Han, D.-H., 1986, Effects of porosity and clay content on acoustic properties of sandstones and unconsolidated sediments: Ph.D. thesis, Stanford University.
- Hatchell, P. and S. Bourne, 2005, Rocks under strain: Strain–induced time–lapse time shifts are observed for depleting reservoirs: *The Leading Edge*, **24**, 1222–1225.
- He, T., 2006, P– and S–wave velocity measurement and pressure sensitivity analysis of AVA response: Master’s thesis, University of Alberta.

- Hemings, D., 2007, Laboratory determination of seismic anisotropy in sedimentary rock from the Western Canadian Sedimentary Basin: Master's thesis, University of Alberta.
- Herwanger, J. and S. Horne, 2005, Predicting time-lapse stress effects in seismic data: *The Leading Edge*, **12**, 1234–1242.
- Jizba, D., 1991, Mechanical and acoustical properties of sandstones and shales: Ph.D. thesis, Stanford University.
- Johnston, J. and N. Christensen, 1995, Seismic anisotropy of shales: *Journal of Geophysical Research*, **100**, no. B4, 5991–6003.
- Kendall, J.-M., Q. Fisher, S. Crump, J. Maddock, A. Carter, S. Hall, J. Wookey, S. Valcke, M. Casey, G. Lloyd, and W. Ismail, 2007, Seismic anisotropy as an indicator of reservoir quality in siliciclastic rocks: Structurally complex reservoirs, 123–136.
- King, M., 1966, Wave velocities in rocks as a function of changes in overburden pressure and pore fluid saturants: *Geophysics*, **31**, no. 1, 50–73.
- King, M., 2002, Elastic wave propagation in and permeability for rocks with multiple parallel fractures: *International Journal of Rock Mechanics and Mining Sciences*, **39**, 1033–1043.
- Lubbe, R., J. Sothcott, M. Worthington, and C. McCann, June 2007, Laboratory estimates of normal/shear fracture compliance ratio Laboratory estimates of normal/shear fracture compliance ratio, European Association of Geoscientists and Engineers 69th Conference & Exhibition, F026.
- Lubbe, R., J. Sothcott, M. Worthington, and C. McCann, 2008, Laboratory estimates of normal and shear fracture compliance: *Geophysical Prospecting*, **56**, 239–247.
- MacBeth, C. and H. Schuett, 2007, The stress dependent elastic properties of thermally induced microfractures in aeolian Rotliegend sandstone: *Geophysical Prospecting*, **55**, 323–332.
- MacBeth, C., 2004, A classification for the pressure-sensitivity properties of a sandstone rock frame: *Geophysics*, **69**, no. 2, 497–510.
- Maddock, J., 2006, Seismic anisotropy in siliciclastic reservoir rocks: Ph.D. thesis, Leeds.
- Nur, A. and G. Simmons, 1969, The effect of saturation on velocity in low porosity rocks: *Earth and Planetary Science Letters*, **7**, 183–193.
- Olden, P., P. Corbett, R. Westerman, J. Somerville, B. Smart, and N. Koutsabeloulis, 2001, Modeling combined fluid and stress change effects in the seismic response of a producing hydrocarbon reservoir: *The Leading Edge*, **20**, no. 10, 1154–1163.
- Palciauskas, V., 1992, Compressional to shear wave velocity ratio of granular rocks: role of rough grain contacts: *Geophysical Research Letters*, **19**, no. 16, 1683–1686.
- Prioul, R., A. Bakulin, and V. Bakulin, 2004, Nonlinear rock physics model for estimation of 3D subsurface stress in anisotropic formations: Theory and laboratory verification: *Geophysics*, **69**, 415–425.

- Raymer, D., A. Tommasi, and J.-M. Kendall, 2000, Predicting the seismic implications of salt anisotropy using numerical simulations of halite deformation: *Geophysics*, **65**, 1272–1280.
- Rojas, M., 2005, Elastic rock properties of tight gas sandstones for reservoir characterization at Rulison Field, Colorado: Master's thesis, Colorado School of Mines.
- Sayers, C. and D.-H. Han, 2002, The effect of pore fluid on the stress-dependent elastic wave velocities in sandstones: *72nd Annual International Meeting, Society of Exploration Geophysicists, Expanded Abstracts*, pages 1842–1845.
- Sayers, C. and M. Kachanov, 1995, Microcrack-induced elastic wave anisotropy of brittle rocks: *Journal of Geophysical Research*, **100**, 4149–4156.
- Sayers, C., 2002, Stress-dependent elastic anisotropy of sandstones: *Geophysical Prospecting*, **50**, 85–95.
- Schoenberg, M. and C. Sayers, 1995, Seismic anisotropy of fractured rock: *Geophysics*, **60**, no. 1, 204–211.
- Schubnel, A. and Y. Guéguen, 2003, Dispersion and anisotropy of elastic waves in cracked rocks: *Journal of Geophysical Research*, **108**, no. B2, 15.
- Shapiro, S. and A. Kaselow, 2005, Porosity and elastic anisotropy of rocks under tectonic stress and pore-pressure changes: *Geophysics*, **70**, N27–N38.
- Shapiro, S., 2003, Elastic piezosensitivity of porous and fractured rocks: *Geophysics*, **68**, 482–486.
- Simmons, G. and W. Brace, 1965, Comparison of static and dynamic measurements of compressibility of rocks: *Journal of Geophysical Research*, **70**, no. 22, 5649–5656.
- Tod, S., 2002, The effects of stress and fluid pressure on the anisotropy of interconnected cracks: *Geophysical Journal International*, **149**, 149–156.
- Valcke, S., M. Casey, G. Lloyd, J.-M. Kendall, and Q. Fisher, 2006, Lattice preferred orientation and seismic anisotropy in sedimentary rocks: *Geophysical Journal International*, **166**, 652–666.
- Van Den Abeele, K. E.-A., J. Carmeliet, P. A. Johnson, and B. Zinszner, 2002, Influence of water saturation on the nonlinear elastic mesoscopic response in earth materials and the implications to the mechanism of nonlinearity: *Journal of Geophysical Research*, **107**, no. B6, 2121.
- Verdon, J., D. Angus, J.-M. Kendall, and S. Hall, 2008, The effects of microstructure and nonlinear stress on anisotropic seismic velocities: *Geophysics*, **73**, no. 4, D41–D51.
- Walsh, J., 1965a, The effect of cracks on the compressibility of rock: *Journal of Geophysical Research*, **70**, 381–389.
- 1965b, The effect of cracks on the uniaxial elastic compression of rocks: *Journal of Geophysical Research*, **70**, 399–411.

Wessel, P. and W. Smith, 1991, Free software helps map and display data: EOS Transactions, **72**, 445–446.

Worthington, M., July 2008, Interpreting seismic anisotropy in fractured reservoirs: First Break, **26**, 29–35.

Zimmerman, R., W. Somerton, and M. King, 1986, Compressibility of porous rocks: Journal of Geophysical Research, **91**, 12765–12777.

## Table Captions

**Table 1.** Published stress core data for various lithologies. Superscript † indicates PhD thesis and \* MSc thesis results.

**Table 2.** Summary of  $\bar{\epsilon}^0$  and  $\bar{a}^0$  estimated for each lithologies after inverting for  $\alpha_{ij}$  only.

**Table 3.** Rock properties of Clair sandstone samples with % of modal constituents [qrtz=quartz, feld=feldspars, calc/dolo=calcite/dolomite and phyllo=phyllosilicates (from Table C.1 Maddock, 2006), and mean estimated initial crack density and initial aspect ratio for inversions using  $\alpha_{ij}$  only (top) and  $\alpha_{ij}$  and  $\beta_{ijkl}$  (bottom).

**Table 4.** Summary of  $\bar{\epsilon}^0$  and  $\bar{a}^0$  estimated for each lithology after inverting for  $\alpha_{ij}$  and  $\beta_{ijkl}$ .

## Figure Captions

**Figure 1.** Flow chart highlighting the inversion procedure for the scalar crack and joint inversions.

**Figure 2.** Comparison of initial crack density ( $\epsilon^0$ ) vs initial aspect ratio ( $a^0$ ) for dry core samples for all lithologies after inverting for  $\alpha_{ij}$  only: anhydrite (black square), carbonate (black inverted triangle), conglomerate (black diamond), dolostone (black circle), limestone (black triangle), sandstone (gray inverted triangle), shale (gray star), tight-gas sandstone (gray diamond), tight-gas shale (gray circle) and Clair sandstone (gray triangle). Inset (as well as in Figs. 3, 5 and 6) are histograms for both  $\epsilon^0$  and  $a^0$ .

**Figure 3.** Comparison of initial crack density ( $\epsilon^0$ ) vs initial aspect ratio ( $a^0$ ) for (a) dry sandstone cores and (b) shale rich cores after inverting for  $\alpha_{ij}$  only (see Fig. 2 for symbol labelling). The Clair sandstones are labelled B, C, D, E, F and I (see Table 3 for petrophysical details).

**Figure 4.** Back-scatter electron images of Clair sandstone samples: clean sandstone samples F [a], I [c], and clay rich sandstone sample C [b and d] (from Maddock, 2006).

**Figure 5.** Comparison of initial crack density ( $\epsilon^0$ ) vs initial aspect ratio ( $a^0$ ) for dry core samples for all lithologies after inversion for both  $\alpha_{ij}$  and  $\beta_{ijkl}$  (see Fig. 2 for symbol labelling).

**Figure 6.** Comparison of initial crack density ( $\epsilon^0$ ) vs initial aspect ratio ( $a^0$ ) for (a) dry sandstone cores and (b) shale rich cores after inverting for  $\alpha_{ij}$  and  $\beta_{ijkl}$  (see Fig. 2 for symbol labelling).

**Figure 7.** Frequency histograms of inverted  $B_N/B_T$  ratios for all lithologies (gray shaded), sandstone samples (blue outline) and carbonate samples (red outline).

**Figure 8.** Frequency histograms for inverted  $B_N/B_T$  ratios for sandstone and tight-gas sandstone lithologies: sandstone samples (gray shaded), tight-gas samples from Rojas (2005) (red outline) and tight-gas samples from Jizba (1991) (blue outline).

**Figure 9.** Frequency histograms for inverted  $B_N/B_T$  ratios for shale lithologies: all shale samples (gray shaded), Hemsing (2007) shale samples (red) and Jizba (1991) tight-gas shale samples (blue).

**Figure 10.** Frequency histograms of inverted  $B_N/B_T$  ratios for undamaged (gray shaded) and damaged (red outline) aeolian Rotliegend sandstone samples from MacBeth and Schuett (2007).

**Figure 11.** Comparison of absolute errors from inversion of synthetic data set for (a) initial crack density  $\epsilon^0$  and (b) initial aspect ratio  $a^0$  for scalar crack inversion (black symbols) and joint inversion (gray symbols). Symbols are for  $(\epsilon^0, a^0)$  sets (0.1,0.0005) [square], (0.5,0.0005) [inverted triangle], (0.1,0.001) [star] and (0.5,0.001) [diamond].

Lithology	Study
Sandstone	King (1966, 2002), Rojas (2005)*, He (2006)*, MacBeth and Schuett (2007), Hemsing (2007)*, Grochau and Gurevich (2008), Hall et al. (2008)
Tight-gas Sandstone	Jizba (1991) <sup>†</sup>
Shale	Johnston and Christensen (1995), Hemsing (2007)*
Tight-gas Shale	Jizba (1991) <sup>†</sup>
Limestone	Simmons and Brace (1965), Nur and Simmons (1969), Brown (2002)*
Dolostone	Nur and Simmons (1969), Brown (2002)*
Conglomerate	He (2006)*
Carbonates/Anhydrites	Hemsing (2007)*

Table 1: Published stress core data for various lithologies. Superscript <sup>†</sup> indicates PhD thesis and \* MSc thesis results.

Parameter	All lithologies	Sandstones	Shales	Carbonates	Tight-gas sandstones
$\bar{\epsilon}^0$	0.1200	0.1550	0.0350	0.0829	0.1500
$\bar{a}^0$	0.0004	0.0004	0.0008	0.0005	0.0004

Table 2: Summary of  $\bar{\epsilon}^0$  and  $\bar{a}^0$  estimated for each lithologies after inverting for  $\alpha_{ij}$  only.

Sample	Depth (m)	Porosity (%)	Permeability (mD)	Qrtz (%)	Felds (%)	Calc/Dolo (%)	Phyllo (%)	$\bar{\epsilon}^0$	$\bar{a}^0$
B	1784	12.0	24.00	38.64	18.26	18.26	12.85	0.0467 0.3983	0.0004 0.0001
C	1788	8.0	0.02	30.89	25.41	1.32	34.38	0.0650 0.1333	0.0008 0.0008
D	1841	11.0	0.07	30.97	21.77	5.92	30.24	0.0217 0.0083	0.0002 0.0099
E	1909	13.0	2.80	54.95	16.07	10.48	5.51	0.1150 0.0833	0.0006 0.0014
F	1950	14.8	84.00	44.19	30.46	7.45	3.10	0.0417 0.0433	0.0003 0.0003
I	2194	12.1	1.40	61.05	12.62	8.06	6.18	0.2550 0.1450	0.0006 0.0005

Table 3: Rock properties of Clair sandstone samples with % of modal constituents [qrtz=quartz, feld=feldspars, calc/dolo=calcite/dolomite and phyllo=phyllosilicates (from Table C.1 Maddock, 2006), and mean estimated initial crack density and initial aspect ratio for inversions using  $\alpha_{ij}$  only (top) and  $\alpha_{ij}$  and  $\beta_{ijkl}$  (bottom).

Parameter	All lithologies	Sandstones	Shales	Carbonates	Tight-gas sandstones
$\bar{\epsilon}^0$	0.1100	0.1300	0.0200	0.1394	0.1100
$\bar{a}^0$	0.0004	0.0004	0.0010	0.0005	0.0004

Table 4: Summary of  $\bar{\epsilon}^0$  and  $\bar{a}^0$  estimated for each lithology after inverting for  $\alpha_{ij}$  and  $\beta_{ijkl}$ .

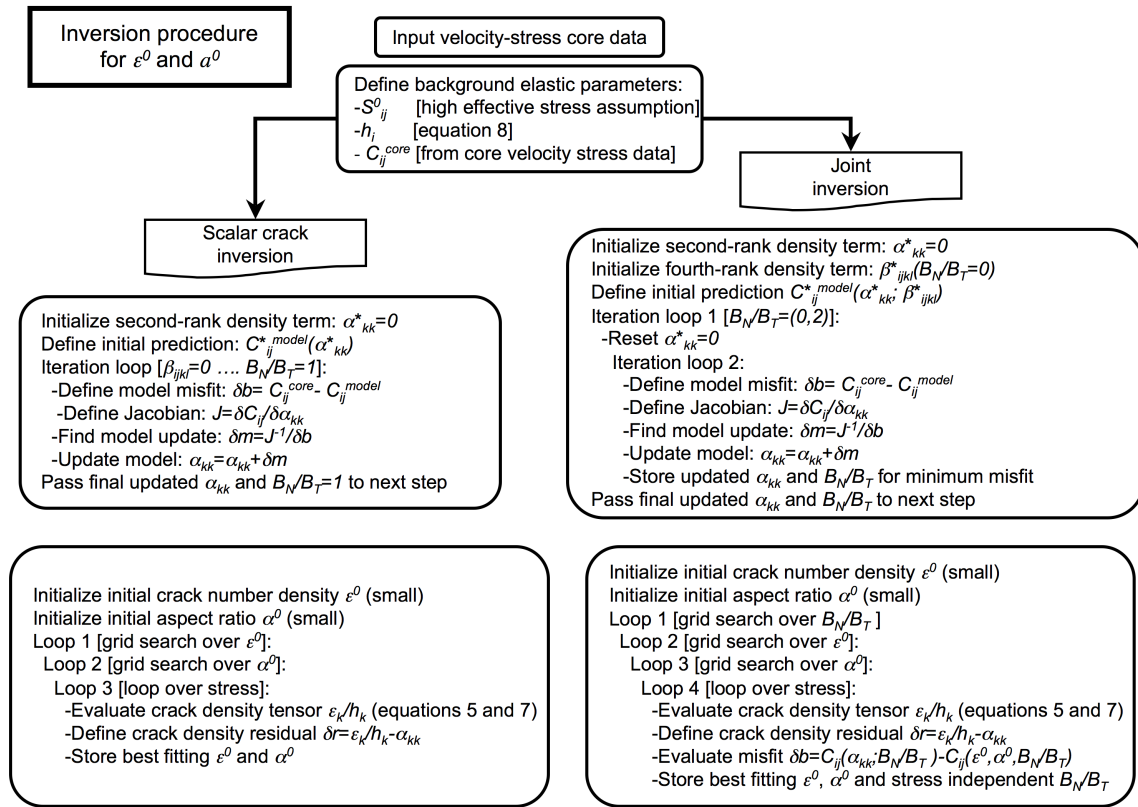


Figure 1: Flow chart highlighting the inversion procedure for the scalar crack and joint inversions.

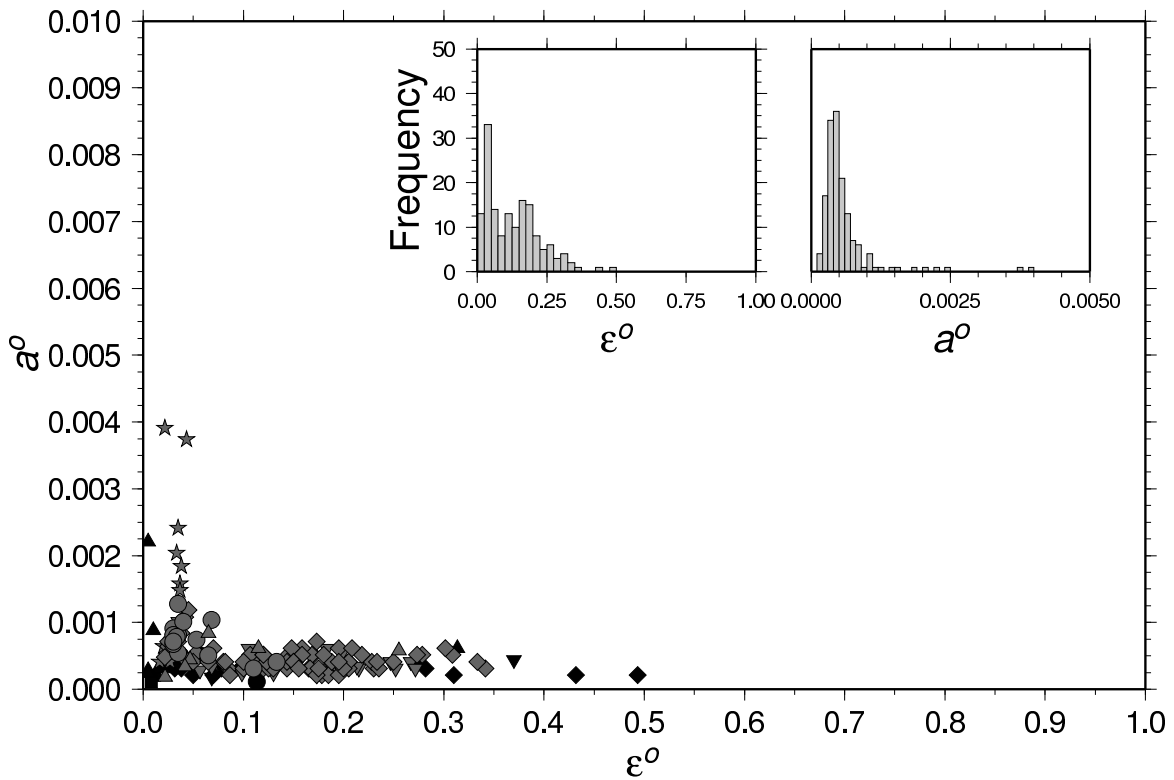


Figure 2: Comparison of initial crack density ( $\epsilon^0$ ) vs initial aspect ratio ( $a^0$ ) for dry core samples for all lithologies after inverting for  $\alpha_{ij}$  only: anhydrite (black square), carbonate (black inverted triangle), conglomerate (black diamond), dolostone (black circle), limestone (black triangle), sandstone (gray inverted triangle), shale (gray star), tight-gas sandstone (gray diamond), tight-gas shale (gray circle) and Clair sandstone (gray triangle). Inset (as well as in Figs. 3, 5 and 6) are histograms for both  $\epsilon^0$  and  $a^0$ .

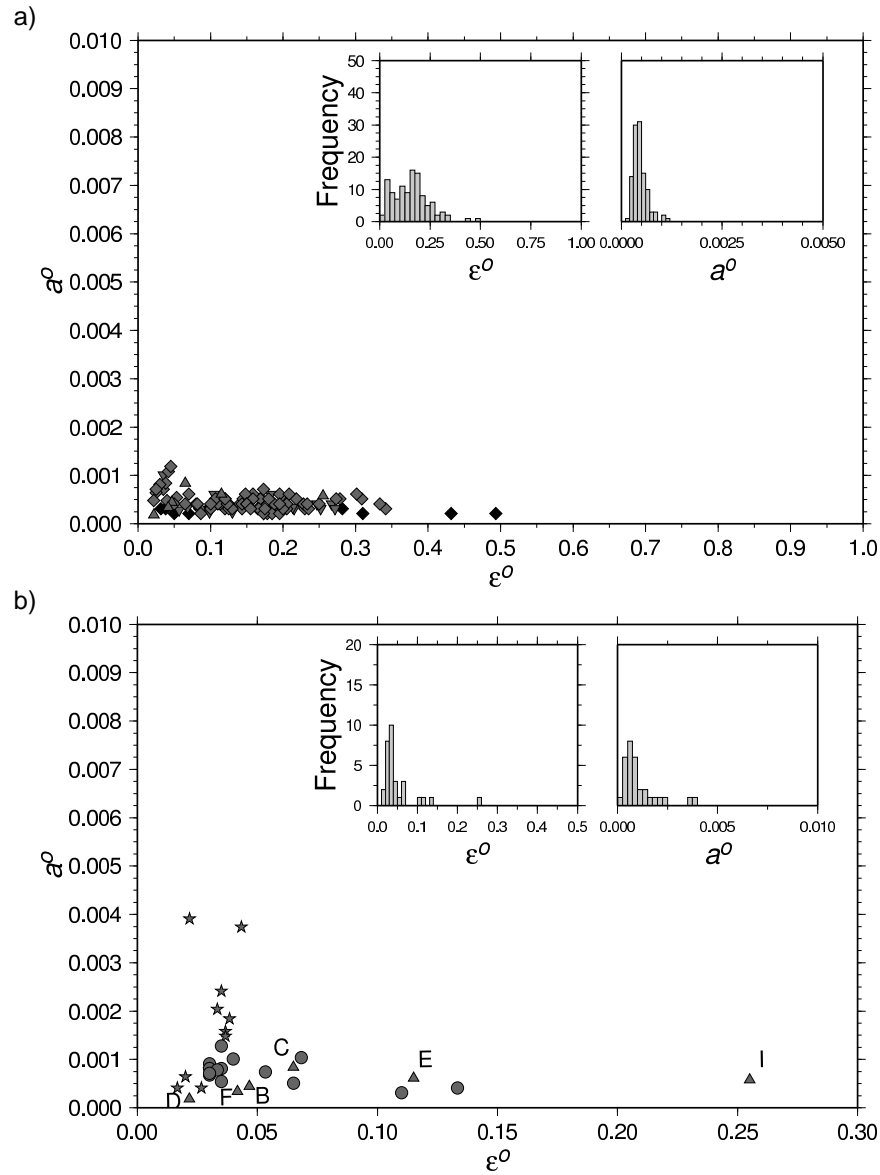


Figure 3: Comparison of initial crack density ( $\epsilon^0$ ) vs initial aspect ratio ( $a^0$ ) for (a) dry sandstone cores and (b) shale rich cores after inverting for  $\alpha_{ij}$  only (see Fig. 2 for symbol labelling). The Clair sandstones are labelled B, C, D, E, F and I (see Table 3 for petrophysical details).

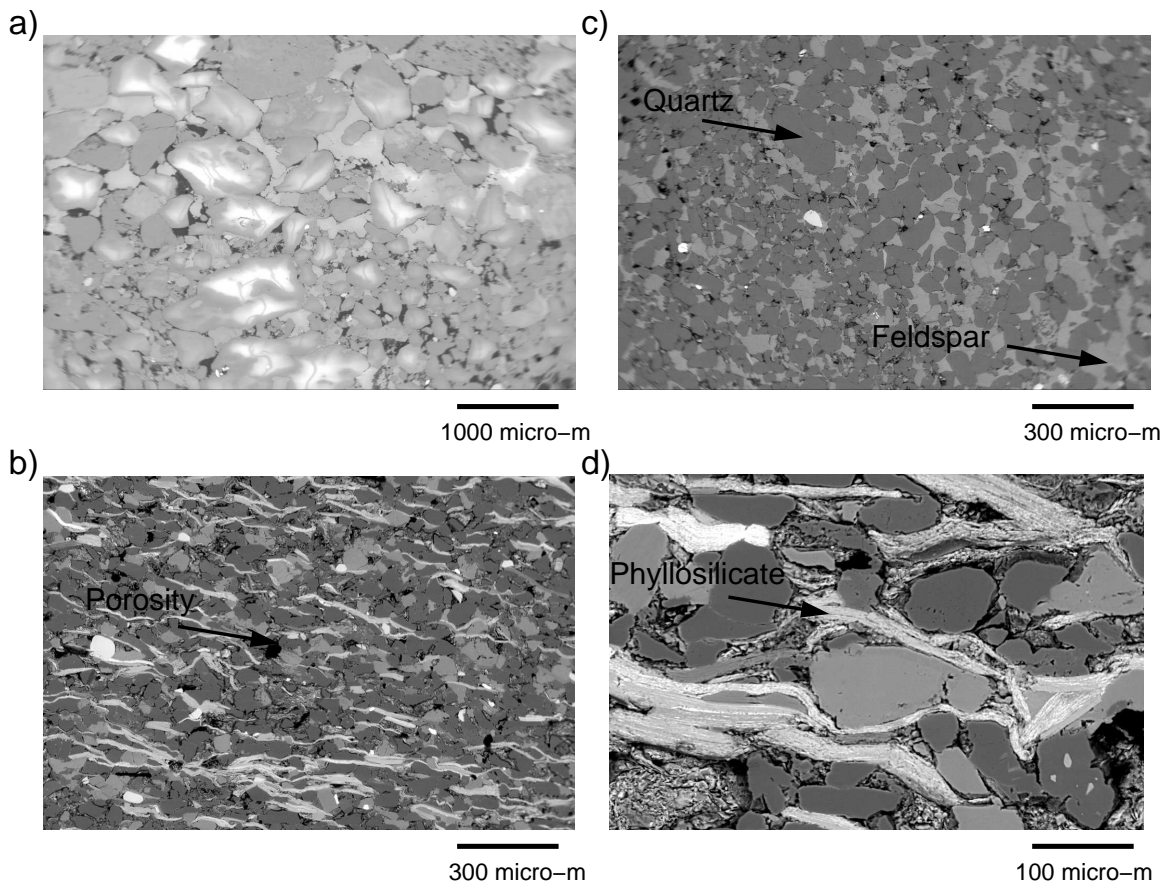


Figure 4: Back-scatter electron images of Clair sandstone samples: clean sandstone samples F [a], I [c], and the clay rich sandstone sample C [b and d] (from Maddock, 2006).

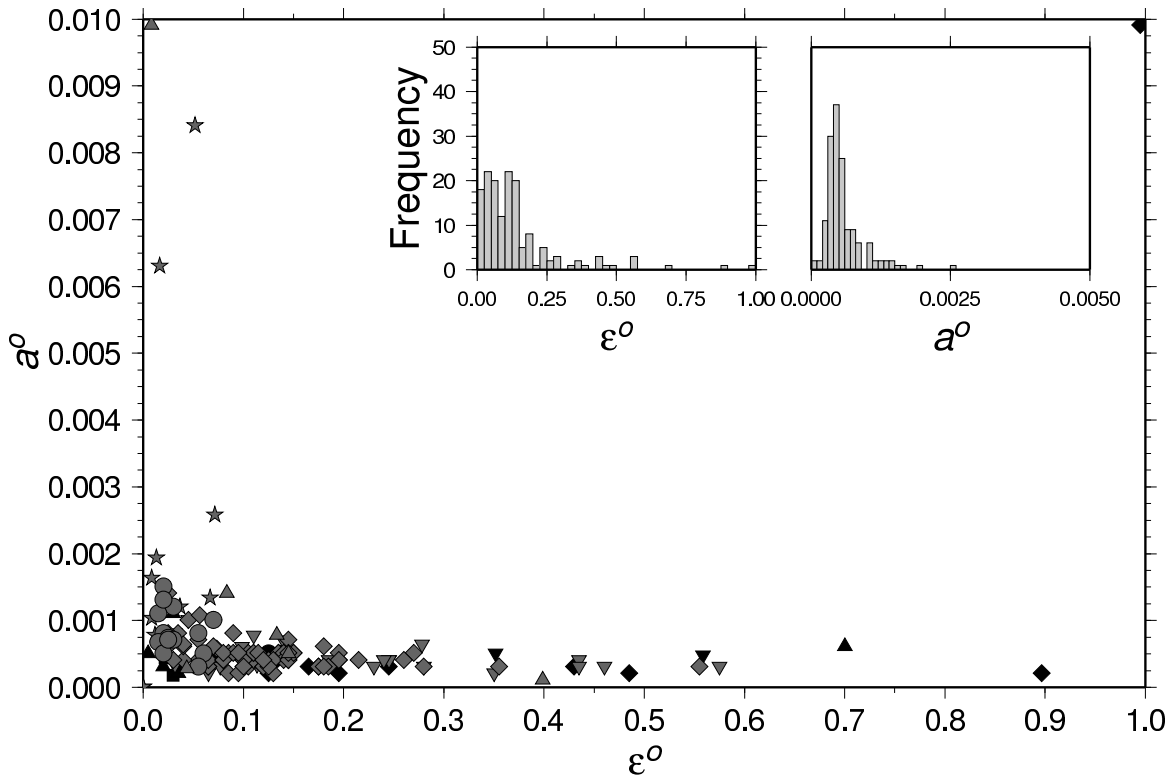


Figure 5: Comparison of initial crack density ( $\epsilon^0$ ) vs initial aspect ratio ( $a^0$ ) for dry core samples for all lithologies after inversion for both  $\alpha_{ij}$  and  $\beta_{ijkl}$  (see Fig. 2 for symbol labelling).

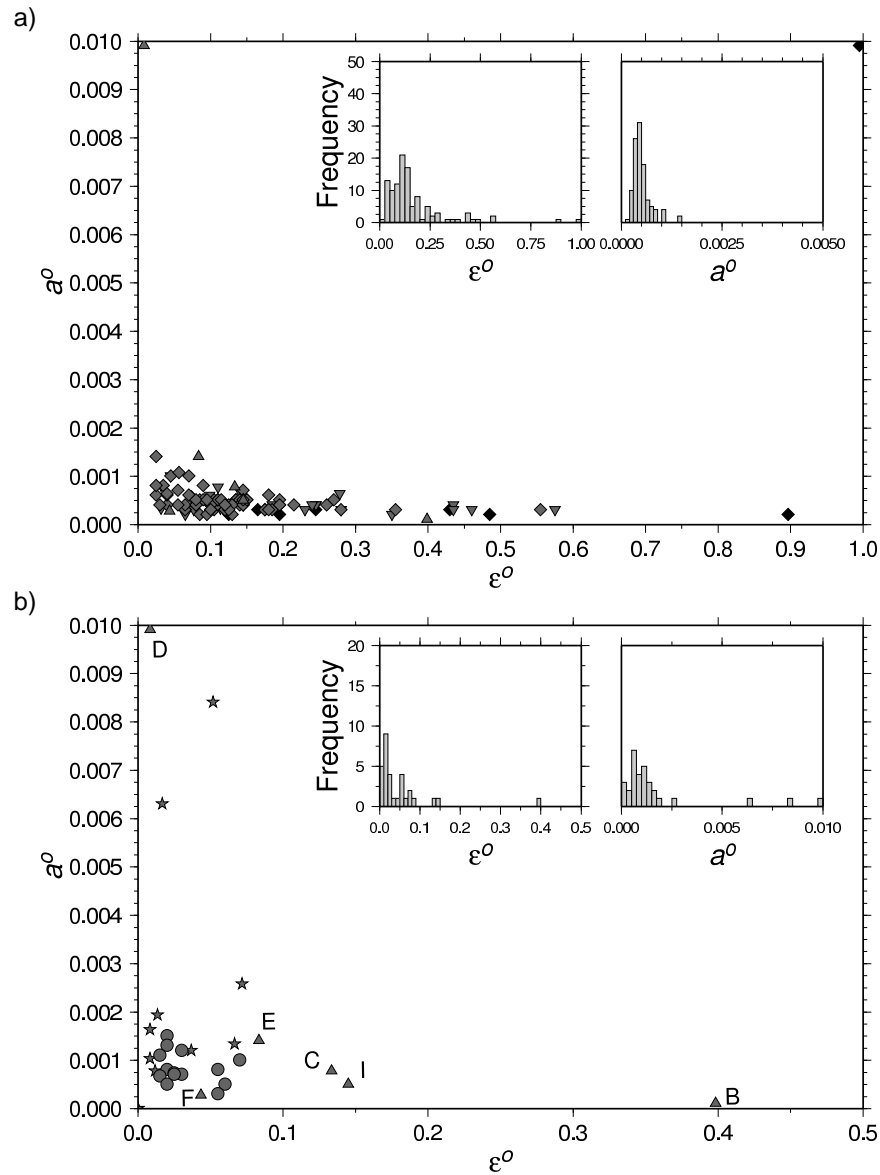


Figure 6: Comparison of initial crack density ( $\epsilon^0$ ) vs initial aspect ratio ( $a^0$ ) for (a) dry sandstone cores and (b) shale rich cores after inverting for  $\alpha_{ij}$  and  $\beta_{ijkl}$  (see Fig. 2 for symbol labelling).

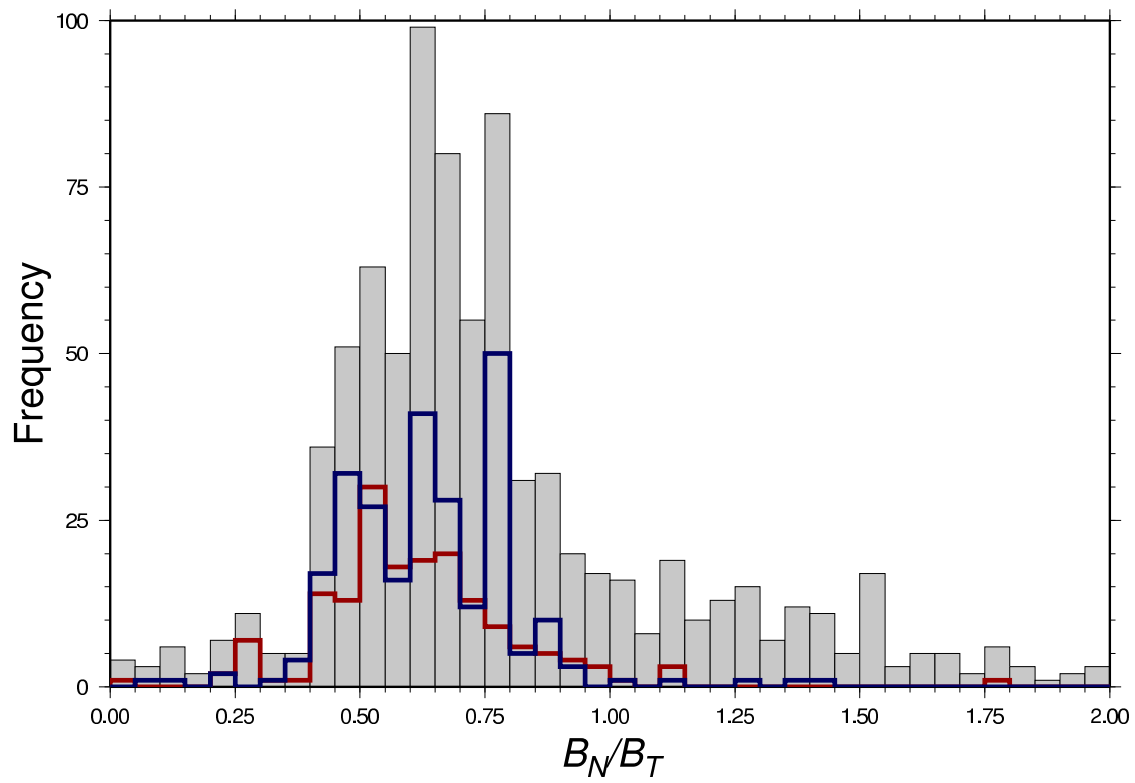


Figure 7: Frequency histograms of inverted  $B_N/B_T$  ratios for all lithologies (gray shaded), sandstone samples (blue outline) and carbonate samples (red outline).

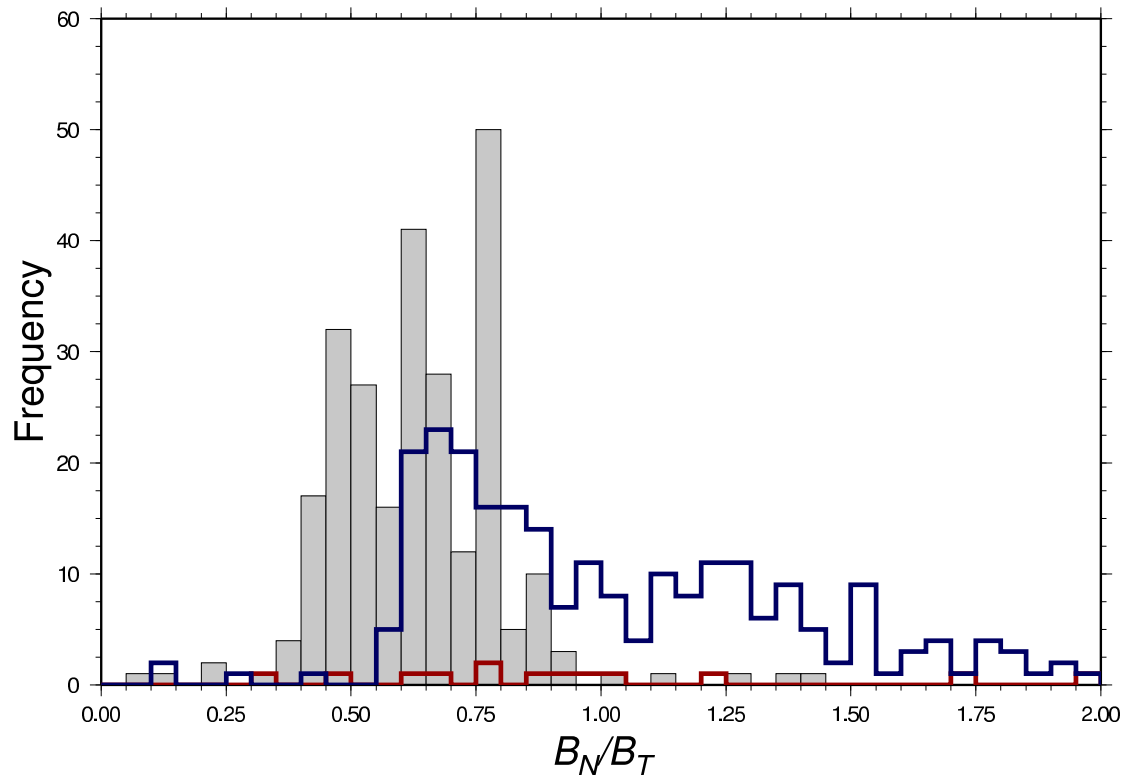


Figure 8: Frequency histograms for inverted  $B_N/B_T$  ratios for sandstone and tight-gas sandstone lithologies: sandstone samples (gray shaded), tight-gas samples from Rojas (2005) (red outline) and tight-gas samples from Jizba (1991) (blue outline).

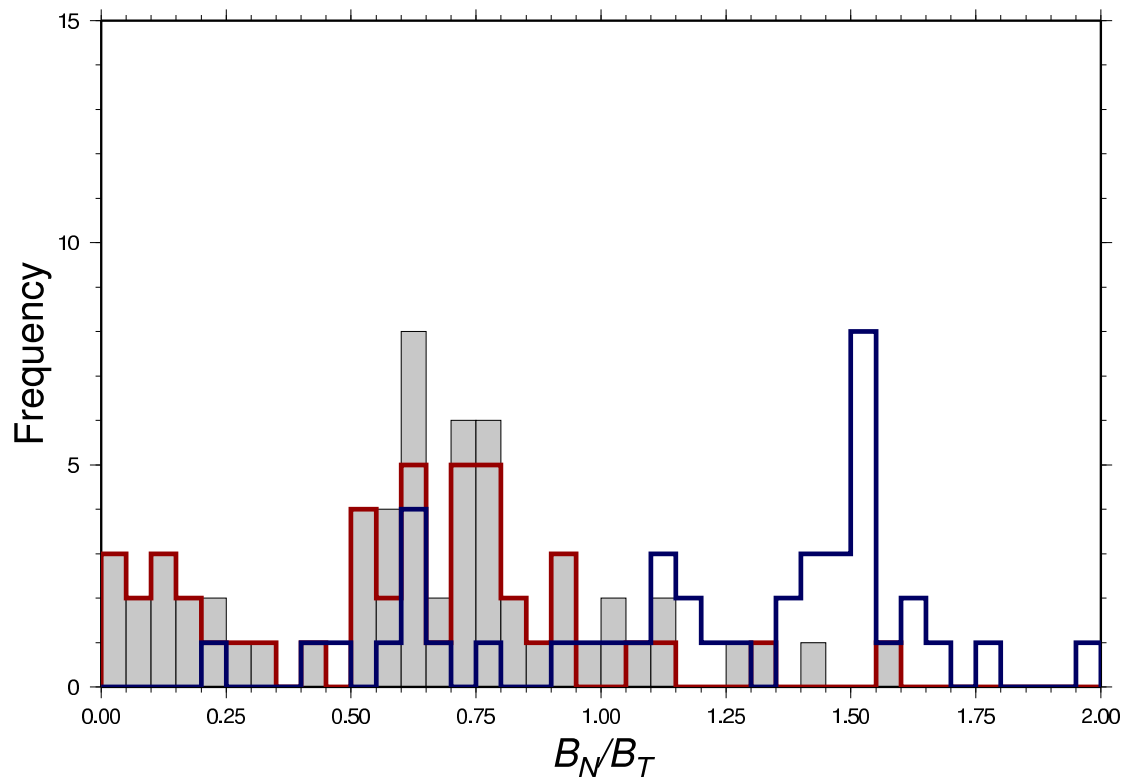


Figure 9: Frequency histograms for inverted  $B_N/B_T$  ratios for shale lithologies: all shale samples (gray shaded), Hemsing (2007) shale samples (red) and all tight-gas shale samples (blue).

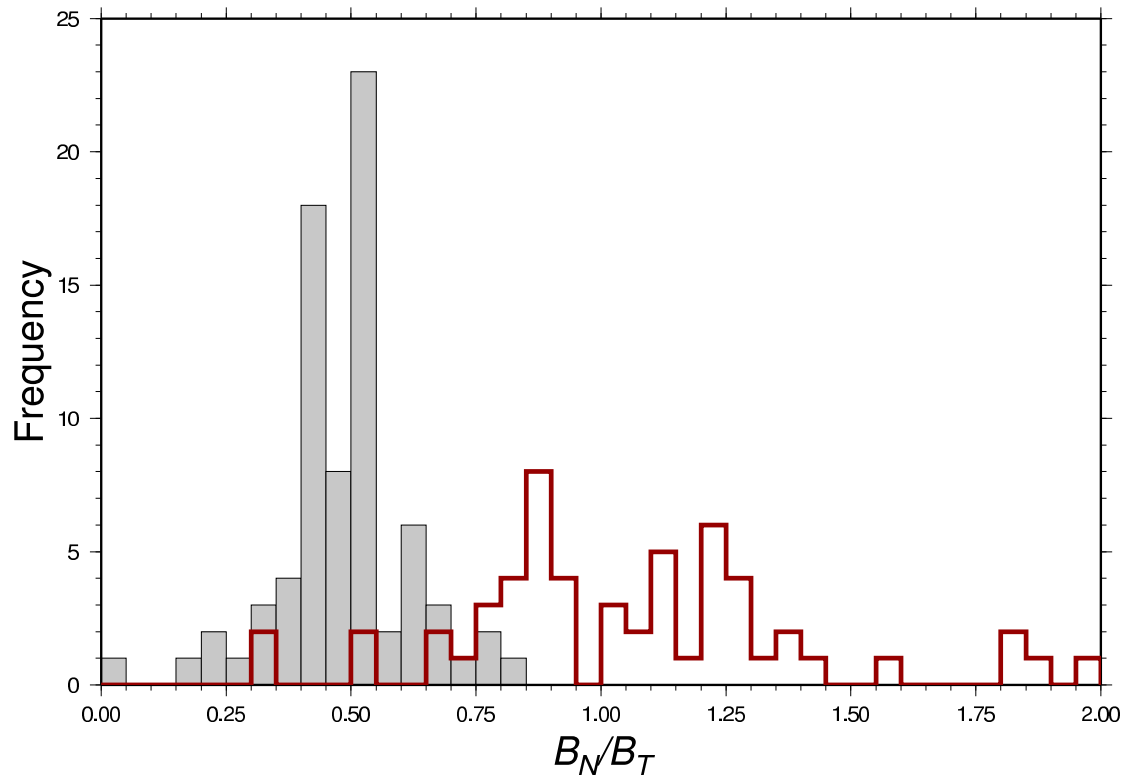


Figure 10: Frequency histograms of inverted  $B_N/B_T$  ratios for undamaged (gray shaded) and damaged (red outline) aeolian Rotliegend sandstone samples from MacBeth and Schuett (2007).

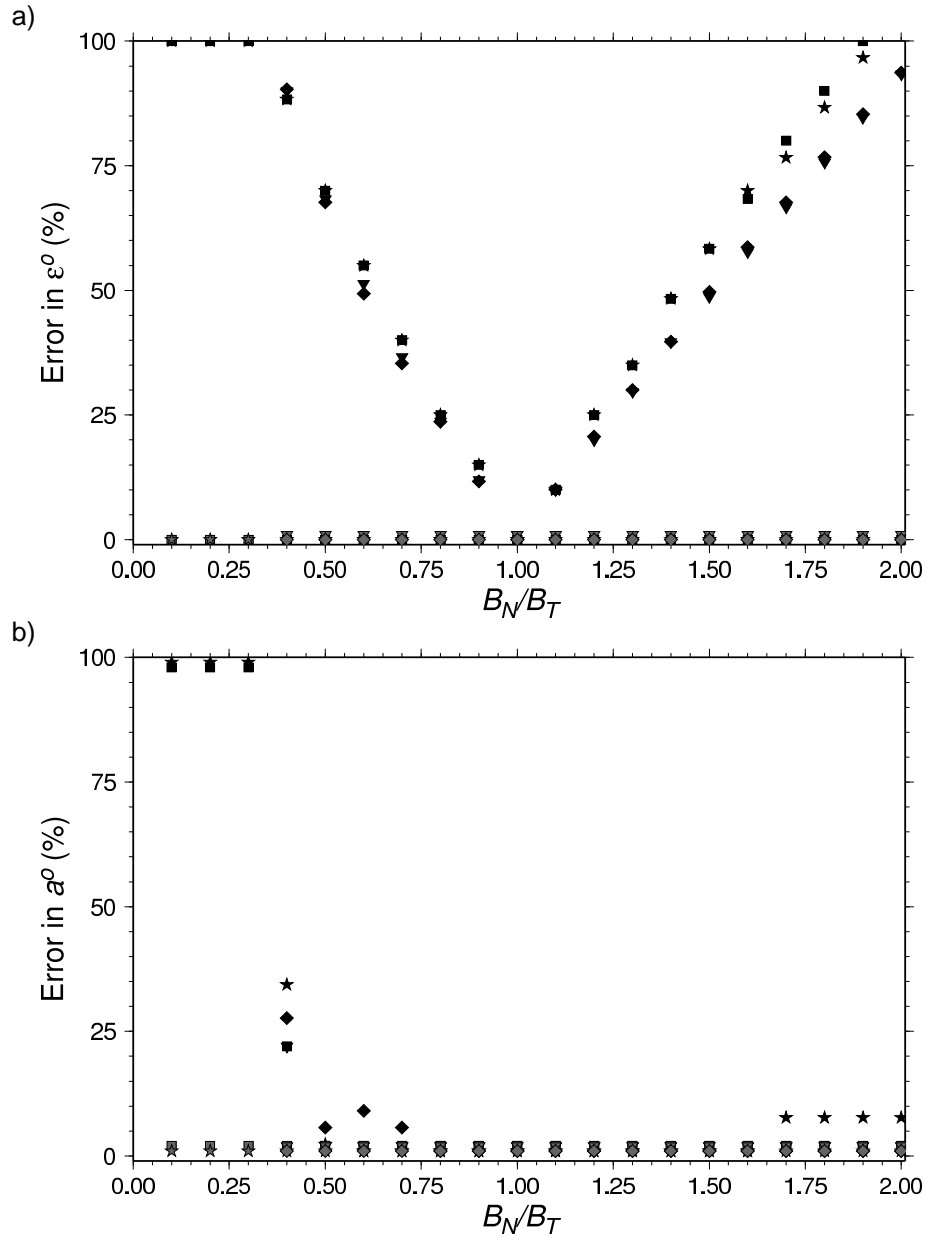


Figure 11: Comparison of absolute errors from inversion of synthetic data set for (a) initial crack density  $\epsilon^0$  and (b) initial aspect ratio  $a^0$  for scalar crack inversion (black symbols) and joint inversion (gray symbols). Symbols are for  $(\epsilon^0, a^0)$  sets (0.1,0.0005) [square], (0.5,0.0005) [inverted triangle], (0.1,0.001) [star] and (0.5,0.001) [diamond].